

Physical properties, crystallization kinetics, and spherulitic growth of well-defined poly(ϵ -caprolactone)s with different arms

Jing-Liang Wang, Chang-Ming Dong *

Department of Polymer Science and Engineering, School of Chemistry and Chemical Technology, Shanghai Jiao Tong University, Shanghai 200240, People's Republic of China

Received 29 August 2005; received in revised form 13 February 2006; accepted 19 February 2006

Available online 27 March 2006

Abstract

Both well defined star-shaped poly(ϵ -caprolactone) having four arms (4sPCL) and six arms (6sPCL) and linear PCL having one arm (LPCL) and two arms (2LPCL) were synthesized and then used for the investigation of physical properties, isothermal and nonisothermal crystallization kinetics, and spherulitic growth. The maximal melting point, the cold crystallization temperature, and the degree of crystallinity of these PCL polymers decrease with the increasing number of polymer arms, and they have similar crystalline structure. The isothermal crystallization rate constant (K) of these PCL polymers is in the order of $K_{2LPCL} > K_{LPCL} > K_{4sPCL} > K_{6sPCL}$. Notably, the K of linear PCL decreases with the increasing molecular weight of polymer while that of star-shaped PCL inversely increases. The variation trend of K over the number of polymer arms or the molecular weight of polymer is consistent with the analyses of both nonisothermal crystallization kinetics and the spherulitic growth rate. These results indicate that both the number of polymer arms and the molecular weight of polymer mainly controlled the isothermal and nonisothermal crystallization rate constants, the spherulitic growth rate, and the spherulitic morphology of these PCL polymers.

© 2006 Elsevier Ltd. All rights reserved.

Keywords: Poly(caprolactone) with different arms; Crystallization kinetics; Spherulitic growth

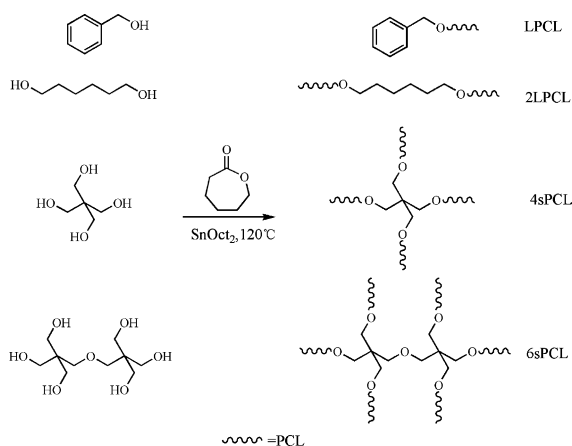
1. Introduction

Owing to their biodegradability, high drug permeability, and biocompatibility, poly(ϵ -caprolactone) (PCL) and the PCL-based blends and copolymers are increasingly investigated worldwide for pharmacological, biomedical, agricultural, and environmental purposes [1–5]. However, as the matrices for drug delivery systems and the scaffolds for tissue engineering, its *in vitro* and/or *in vivo* degradation rate is very slow and usually cannot be controlled because of its high crystallinity and the hydrophobicity of polymer back-bone. Significantly, the promising approaches to solve these problems are mainly investigated from several aspects, for examples, the adjustment of polymer hydrophilicity–hydrophobicity balance, the copolymer or polymer blend with polylactides and poly lactones, and the control of branched macromolecular architectures [6–10]. The branched polymers such as star-shaped polymers, hyperbranched polymers, and

dendrimers have attracted much attention in the past decades because of their useful rheological and mechanical properties, and ease of control of surface functionality, which are not accessible in conventional linear polymers [11–15].

Recently, star-shaped PCL with well-defined architectures have been extensively investigated by different research groups using multifunctional small molecules and/or dendritic molecules. For examples, Hedrick et al. reported the synthesis of dendrimer-like and layered triblock PCL polymers using a hexahydroxy-functional compound initiator and stannous octoate (SnOct_2) catalyst [16–18]. Frechet et al. reported the synthesis and encapsulation properties of porphyrin-based multiarm PCL [19,20]. Kricheldorf et al., Sanda et al., and Qiu et al. synthesized three- and four-arm star-shaped PCL with a multifunctional initiator such as trimethylolpropane or pentaerythritol, and with $\text{Bi}(\text{OAc})_3$, protonic acid, or SnOct_2 as the catalyst, respectively [21–26]. As an extension, Frey et al. synthesized multiarm PCL block copolymers with hyperbranched polyglycerol as the core [27]. Kwak et al. synthesized an ill-defined hyperbranched PCL and investigated the architectural effect on its crystallization [28,29]. Xi et al. reported the synthesis and thermal properties of star-shaped PAMAM–PLLA hybrid using a dendritic hydroxyl-terminated

* Corresponding author. Tel.: +86 21 54748916; fax: +86 21 54741297.
E-mail address: cmdong@sjtu.edu.cn (C.-M. Dong).



Scheme 1. Synthesis of poly(ϵ -caprolactone) (PCL) with different arms using both commercial primary alcohols and SnOct₂ in bulk at 120 °C.

poly(amidoamine) (PAMAM) macroinitiator, and the dendrimer-like poly(aryl ether)-PLLA hybrid was recently synthesized [30–33]. Wang et al. studied the synthesis and controlled drug release properties of PAMAM-g-PLLA using an amine-terminated PAMAM macroinitiator [8]. Cao et al. reported the preparation and crystallization kinetics of star-shaped PLLA initiated with sugar alcohols [34]. However, it looks to us that the systematic investigation on the physical properties, isothermal and nonisothermal crystallization kinetics, and spherulitic growth and morphology of well-defined PCL with different arms have not been reported. Significantly,

this study on the effects of both the number of polymer arms and the molecular weight of polymer on the properties of these PCLs will shed light on designing new PCL-based materials with novel properties. For this purpose, we have synthesized a series of well-defined PCL with different arms using the core-first approach (Scheme 1), and then their physical properties, crystallization kinetics, and spherulitic growth and morphology were thoroughly investigated based on DSC, WAXD, and POM analyses.

2. Experimental section

2.1. Materials

Stannous octoate (SnOct₂, Aldrich) was used as received. ϵ -Caprolactone (CL, Aldrich), toluene and benzyl alcohol were distilled from CaH₂, respectively. 1,6-Hexanediol, pentaerythritol, and dipentaerythritol were purchased from Aldrich and then dried in vacuo for 24 h. The other reagents and solvents were local commercial products and used without further purification.

2.2. Methods

¹H NMR and ¹³C NMR spectroscopy was performed on a Varian Mercury-400 spectrometer. Tetramethylsilane was used as an internal standard. Molecular weights and molecular weight distributions of the polymers were determined on a Waters 717 plus autosampler gel permeation chromatograph

Table 1
Synthesis of poly(ϵ -caprolactone) (PCL) with different arms using commercial primary alcohol as initiator and stannous octoate (SnOct₂) catalyst in bulk at 120 °C

Entry	[M]/[I] ^a	$M_{n,GPC}$ ^b	$M_{n,NMR}$ ^c	$M_{n,th}$ ^d	$M_{n,arm}$ ^e	M_w/M_n ^b	Yield (%)
LPCL1 ^f	60	5980	5980	6450	5980	1.57	93.5
LPCL2 ^f	120	11,500	9500	11,100	11,500	1.13	81.2
LPCL4 ^f	480	–	20,680	49,800	–	–	91.0
2LPCL1 ^g	60	5190	6470	6460	2600	1.12	94.5
2LPCL2 ^g	120	10,410	–	11,690	5210	1.24	85.5
2LPCL3 ^g	186	16,860	–	19,190	8430	1.42	90.6
2LPCL4 ^g	251	20,730	21,850	26,600	10,370	1.53	92.9
4sPCL1 ^h	58	6070	6900	5870	1520	1.07	88.8
4sPCL2 ^h	116	12,540	–	12,330	3140	1.10	93.3
4sPCL3 ^h	176	17,140	–	18,730	4290	1.22	93.3
4sPCL4 ^h	238	18,830	24,560	25,680	4710	1.34	94.6
6sPCL1 ⁱ	58	7160	7650	6120	1190	1.05	92.6
6sPCL2 ⁱ	122	11,820	12,980	12,430	1970	1.08	89.4
6sPCL3 ⁱ	180	13,410	19,720	15,390	2240	1.15	75.0
6sPCL4 ⁱ	237	17,110	28,670	25,780	2850	1.07	95.3

[M]/[SnOct₂] = 1000/1, and the polymerization time = 24 h.

^a M = CL; I = initiator = primary alcohol.

^b Weight-average molecular weight (M_w) and number-average molecular weight (M_n) are determined by GPC.

^c $M_{n,NMR}$ was determined from the integral ratio of the signal on the main chain of polymer (–CH₂, 2.10–2.40 ppm) and the signal on the primary hydroxy methylene end group (HOCH₂, 3.60 ppm).

^d $M_{n,th} = [M]/[I] \times M_{CL} \times \text{yield}$, $M_{n,th}$ denotes the theoretical number-average molecular weight of polymer.

^e $M_{n,arm}$ represents the units of arm length of PCL, and $M_{n,arm} = M_{n,GPC}/\text{polymer arm number}$.

^f LPCL denotes the linear PCL having one arm synthesized using a benzyl alcohol initiator.

^g 2LPCL denotes the linear PCL having two arms synthesized using a 1,6-hexanediol initiator.

^h 4sPCL denotes the star-shaped PCL having four arms synthesized using a pentaerythritol initiator.

ⁱ 6sPCL denotes the star-shaped PCL having six arms, which was synthesized using a dipentaerythritol initiator in Ref. [26].

Table 2
The melting and crystallization behaviors of the PCL polymers with different arms

Entry	T_{m1}^a (°C)	T_{m2}^a (°C)	T_c^b (°C)	ΔH_{m1}^c (J/g)	X_{c1}^d (%)	ΔH_c^e (J/g)	ΔH_{m2}^c (J/g)	X_{c2}^d (%)
LPCL1	58.0	58.0	35.4	92.7	66.4	68.8	93.1	66.7
2LPCL1	55.8	53.8	34.5	115.0	82.4	83.5	85.4	61.2
2LPCL2	56.0	55.1	35.0	111.0	79.5	79.9	81.8	58.6
2LPCL3	58.0	55.8	33.5	90.3	64.7	66.5	66.5	47.7
2LPCL4	59.1	56.5	33.4	99.4	71.3	71.4	68.1	48.8
4sPCL1	50.1	47.2	26.1	95.1	68.2	68.9	71.7	51.4
4sPCL2	53.6	51.8	30.8	112.7	80.8	79.8	79.3	56.8
4sPCL3	56.4	53.8	31.4	97.7	70.0	70.1	67.4	48.3
4sPCL4	59.1	54.9	31.2	93.1	66.7	67.6	64.9	46.5
6sPCL1	48.6	42.9	20.1	81.2	58.2	59.7	56.8	40.7
6sPCL2	54.5	49.8	28.3	85.0	60.9	60.7	55.5	39.7
6sPCL3	55.7	52.6	31.0	106.3	76.2	75.8	72.4	51.9
6sPCL4	57.0	53.0	31.0	86.5	61.9	65.0	64.3	46.1

^a T_{m1} and T_{m2} denote the maximal melting temperature of polymer in the first and second heating run, respectively.

^b T_c denotes the crystallization temperature of polymer in the cooling run.

^c ΔH_{m1} and ΔH_{m2} denote the fusion enthalpy of polymer in the first and second heating run, respectively.

^d $X_{c1} = \Delta H_{m1}/\Delta H_m^0$, $X_{c2} = \Delta H_{m2}/\Delta H_m^0$, $\Delta H_m^0 = 139.6$ J/g.

^e ΔH_c denotes the crystallization enthalpy of polymer in the cooling run.

equipped with Waters RH columns and the DAWN EOS (Wyatt Technology) multiangle laser light-scattering detector at 30 °C, THF as the eluent (1.0 mL/min). The differential scanning calorimetry (DSC) analysis was carried out using a Perkin–Elmer Pyris 1 instrument under nitrogen flow (10 mL/min). For their physical properties, all samples were first heated from -25 to 90 °C at 10 °C/min and held for 3 min to erase the thermal history, then cooled to -25 at 10 °C/min, and finally heated to 90 °C at 10 °C/min. With respect to isothermal crystallization kinetics, the samples were first heated to 90 °C and held for 3 min, and then quenched to the preset crystallization temperature, and the DSC traces were recorded as a function of time. In a similar manner, the samples were heated to 90 °C and held for 3 min, and then cooled to -25 °C at various cooling rates of 2, 6, and 10 °C/min, and the DSC traces were recorded for nonisothermal crystallization kinetics. Wide angle X-ray diffraction (WAXD) patterns of powder samples were obtained at room temperature on a Shimadzu XRD-6000 X-ray diffractometer with a $\text{Cu K}\alpha$ radiation source (wavelength = 1.54 Å). The supplied voltage and current were set to 40 kV and 30 mA, respectively. Samples were exposed at a scan rate of $2\theta = 4^\circ/\text{min}$ between $2\theta = 5$ and 40° . The crystallization morphology of polymer was observed using a Leica DMLP polarized optical microscope (Leica Microsystems GmbH, Germany). The solution of sample in CH_2Cl_2 (4 mg/mL) was sandwiched between two glass plates after the solvent completely evaporated, heated to a temperature 20 °C higher than the maximal melting point, and held for 3 min to erase the thermal history, and then quenched to the preset crystallization temperature.

2.3. Synthesis of poly(ϵ -caprolactone) with different arms

The polymerization tubes were kept at 110 °C for 24 h. CL, the primary alcohol, and a dry stirring bar were put into the warm tube quickly. The tube was then connected to a Schlenk

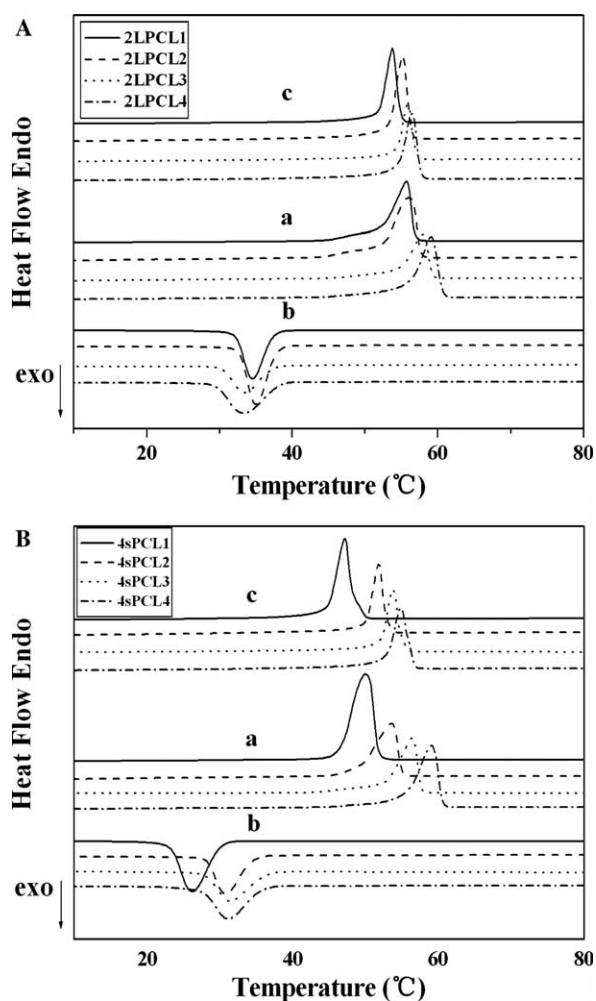


Fig. 1. DSC curves of two-arm linear PCL (2LPCL; A) and four-arm star-shaped PCL (4sPCL; B) in the first heating run (a), in the cooling run (b), and in the second heating run (c), respectively.

line, where an exhausting–refilling process was repeated three times. The tube was put into an oil bath at 120 °C with vigorous stirring for about 5 min. A certain amount of SnOct₂ in dry toluene was added to the melt mixture, and the exhausting–refilling process was carried out again for removal of the toluene. The tube was cooled after the desired reaction time. The resulting product was dissolved in CH₂Cl₂ and poured dropwise into an excess of cold methanol under vigorous stirring. The purified polymer was dried in vacuo until a constant weight was obtained. Then the polymer yield was determined gravimetrically. A typical example follows: 2.88 mg (7.22 μmol) of SnOct₂ catalyst was added to the melt mixture of pentaerythritol (4.1 mg; 0.030 mmol) and CL monomer (824 mg, 7.22 mmol). The polymerization was carried out in bulk at 120 °C for 24 h. Then, the resulting product was dissolved in 10 mL of CH₂Cl₂ and poured dropwise into 100 mL of cold methanol under vigorous stirring at room temperature. The precipitate was filtered and dried in vacuo at 40 °C to give 779.5 mg of the 4sPCL4 sample (94.6 wt% yield).

3. Results and discussion

3.1. Physical properties of well-defined poly(ϵ -caprolactone) with different arms

It is known that biodegradable aliphatic polyesters with well-defined architecture can be synthesized from the

ring-opening polymerization of lactides and/or lactones using a hydroxy-containing compound as initiator and SnOct₂ as catalyst [23–26,31–34]. In order to easily synthesize well-defined PCL with different arms, we chose commercial primary alcohols such as benzyl alcohol, 1,6-hexane alcohol, pentaerythritol, and dipentaerythritol as initiators, and SnOct₂ as the catalyst. The controlled ring-opening polymerization of CL was successfully performed to obtain the model PCL polymers with well-defined architecture, such as star-shaped PCL having four arms (4sPCL) and six arms (6sPCL) and linear PCL having one arm (LPCL) and two arms (2LPCL) (Scheme 1). Based on the analyses of GPC and NMR, the molecular weights of these PCL polymers can be controlled by the molar ratio of CL monomer to the alcohol initiator, and the molecular weight distribution was rather narrow (Table 1). Then these well-defined PCL polymers with similar molecular weights were investigated for their physical properties, isothermal and nonisothermal crystallization kinetics, and spherulitic growth and morphology.

The melting and crystallization behaviors of these PCL polymers are investigated by DSC, and the results are compiled in Table 2. As the representative examples, Fig. 1 shows the DSC curves of 2LPCL and 4sPCL polymers in the first heating run, in the cooling run, and then in the second heating run, respectively. These curves indicate the presence of a few characteristic transitions such as melting and crystallization, which are typical for semicrystalline PCL. All PCL polymers have a monomodal melting peak at $T_{m1} = 48.6$ –59.1 °C in the first heating run, a crystallization point at $T_c = 20.1$ –35.4 °C in

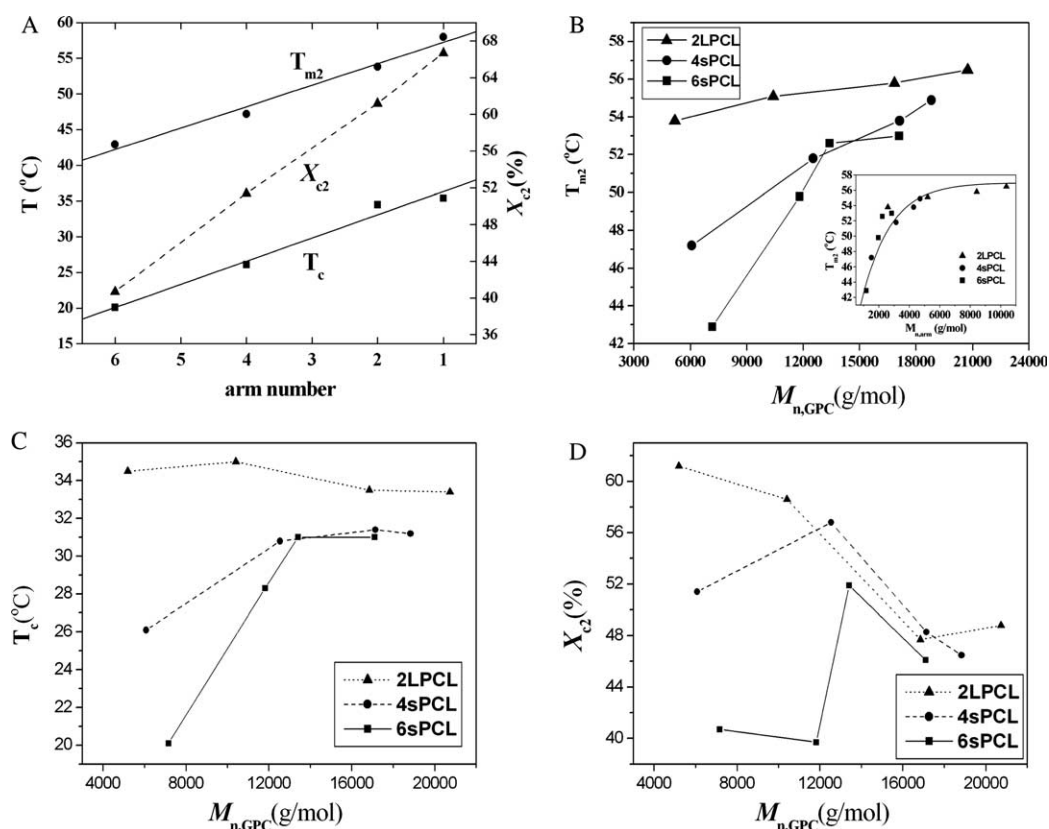


Fig. 2. (A) The dependence of T_{m2} , T_c , and X_{c2} on the arm number of PCL; (B) the dependence of T_m on the molecular weight of PCL; (C) the dependence of T_c on the molecular weight of PCL; (D) the dependence of X_{c2} on the molecular weight of PCL.

the cooling run, and a monomodal endotherm peak at $T_{m2}=42.9\text{--}58.0\text{ }^{\circ}\text{C}$ in the second heating run, respectively. These indicate that the secondary crystallization possibly did not exist in the well-defined PCL polymers, which all had enough time to rearrange and crystallize in the heating and cooling runs because of their low glass transition temperature (about $-60\text{ }^{\circ}\text{C}$) and molecular regularity [29–31]. Moreover, both the maximal melting temperature (T_m) and the crystallization temperature (T_c) decrease with the increasing arm number of PCL, and they are in the order of LPCL > 2LPCL > 4sPCL > 6sPCL (Fig. 2(A)). This is attributed to the decreasing molecular weight of each PCL arm linking to the functional initiator core, which induces the increasing arm density of PCL (arm number per unit mass) [29]. Furthermore, the T_m increases with the increasing molecular weight of polymer, and the variation trend (i.e. the slope of line) is highlighted in star-shaped PCL more than that in linear PCL (Fig. 2(B)). As a note, the actual melting point is determined by the length of the arms ($M_{n,arm}$ in Table 1) and not by the molar mass of the entire molecule, irrespective of the number of arms (see T_m vs $M_{n,arm}$ in Fig. 2(B)). The similar variation trend is also observed for the T_c of star-shaped PCL, while the T_c of linear PCL approximately has no variation over its molecular weight (Fig. 2(C)). This is similar to that reported for 3-arm star-shaped poly(L-lactide)s [35].

Degree of crystallinity (X_c) of these PCL polymers was determined from DSC analysis with the aid of the enthalpy of fusion of 139.6 J/g for the perfectly crystalline PCL [36]. The X_c decreases with the increasing arm number of PCL, and it is in the order of $X_{c,LPCL} > X_{c,2LPCL} > X_{c,4sPCL} > X_{c,6sPCL}$ (Fig. 2(A)). However, the X_c has no obvious dependence on the molecular weight of polymer (Fig. 2(D)). In addition, the X_{c1} value determined in the first heating curve was apparently higher than the X_{c2} value determined in the second heating curve. This indicates that the thermal history has obvious effect on the X_c of the semicrystalline PCL. Notably, the wide angle X-ray diffractograms of both linear and star-shaped PCL polymers showed prominent peaks at ~ 21.0 and ~ 24.0 , which is consistent with that for PCL crystals located at 21.4 and 23.8 [37] (Supporting Information S1). This indicates that the PCL polymers have similar crystalline structure, and both the core initiator and the branch arm structure have no apparent effect on it.

3.2. Isothermal crystallization kinetics

The isothermal crystallization kinetics of these PCL polymers was first investigated by DSC, and the Avrami equation was used to analyze the isothermal crystallization process [29,34,38]. Fig. 3 shows the dependence of relative

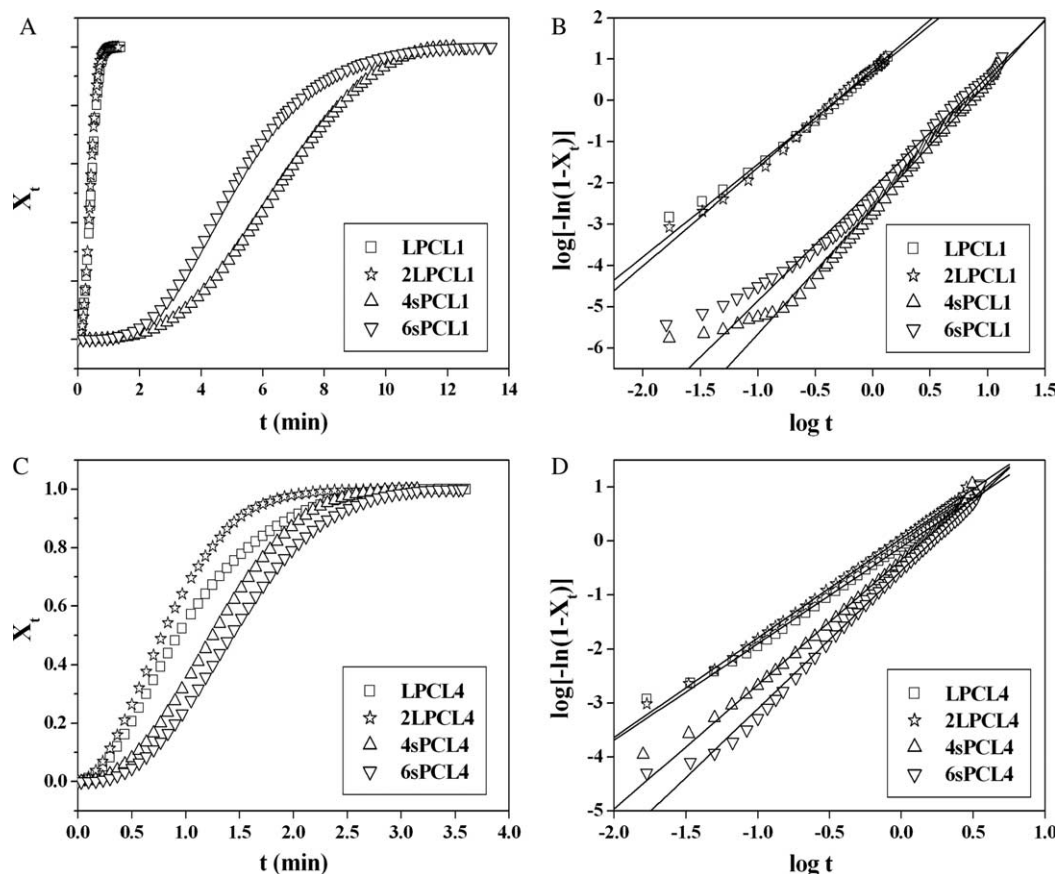


Fig. 3. (A) Plots of relative degree of crystallinity (X_t) vs isothermal crystallization time (t) for the PCL with a low molecular weight; (B) plots of $\log[-\ln(1-X_t)]$ vs $\log t$ for the PCL with a low molecular weight; (C) plots of relative degree of crystallinity (X_t) vs isothermal crystallization time (t) for the PCL with a high molecular weight; (D) plots of $\log[-\ln(1-X_t)]$ vs $\log t$ for the PCL with a high molecular weight.

Table 3
Isothermal crystallization kinetics results for the PCL polymers with different arms

Entry	n^a	K (min^{-n}) ^b	G ($\mu\text{m/s}$) ^c	$t_{1/2}$ ^d
LPCL1	2.2	4.92	0.55	0.42
2LPCL1	2.4	5.70	0.57	0.41
4sPCL1	3.0	2.45×10^{-3}	0.08	6.37
6sPCL1	2.7	7.24×10^{-3}	0.04	5.36
LPCL4	1.8	0.77	0.41	0.94
2LPCL4	1.8	1.10	0.42	0.78
4sPCL4	2.3	0.44	0.35	1.22
6sPCL4	2.5	0.28	0.34	1.29

^a Avrami exponent (n) determined from Fig. 3(B) and (D).

^b Isothermal crystallization rate constant (K) determined from Fig. 3(B) and (D).

^c Spherulitic growth rate (G) determined from Fig. 4(C) and (D).

^d The crystallization half-time ($t_{1/2}$) is defined as the time at which the extent of crystallization is complete by 50%, and $t_{1/2} = (\ln 2/K)^{1/n}$.

degree of crystallization on the crystallization time for the PCL polymers with a low molecular weight and a high molecular weight, respectively. It can be seen that the X_t increases with the increasing crystallization time, and linear PCL crystallized faster than star-shaped PCL analogues (Fig. 3(A) and (C)). Additionally, the plots of $\log[-\ln(1-X_t)]$ vs $\log t$ were also shown in Fig. 3(B) and (D), and the values of the Avrami exponent (n), the isothermal crystallization rate constant (K),

and the crystallization half-time ($t_{1/2}$) are listed in Table 3. Each curve exhibits a good linear relationship, suggesting that the isothermal crystallization kinetics is in good agreement with the Avrami equation. This indicates the secondary crystallization does not exist in these PCL polymers, which is consistent with that concluded from the above DSC analysis. The Avrami exponent varied from 1.8 to 2.4 for both LPCL and 2LPCL, and 2.3 to 3.0 for both 4sPCL and 6sPCL, respectively. This suggests that the crystallization mode of both linear and star-shaped PCL polymers is of two- and/or three-dimensional growth with a heterogeneous nucleation. Moreover, the isothermal crystallization rate constant is in the order of $K_{2LPCL} > K_{LPCL} > K_{4sPCL} > K_{6sPCL}$. This is attributed to the following reasons. For the linear PCL, the molecular mobility increases with both the increasing arm number and the decreasing molecular weight of each arm, which induced that 2LPCL had a higher value of K than LPCL. However, with the continuous increasing arm number, both the strong hydrogen-bond interactions among the arms of star-shaped PCL and the constrained geometry mainly decreased the molecular mobility and rearrangement, suggesting a lower value of K . As a note, it can be seen that the K of linear PCL decreases with the increasing molecular weight of polymer, which also suggests that the molecular mobility is a major factor for its crystallization (Fig. 4(A)). However, the K of star-shaped PCL

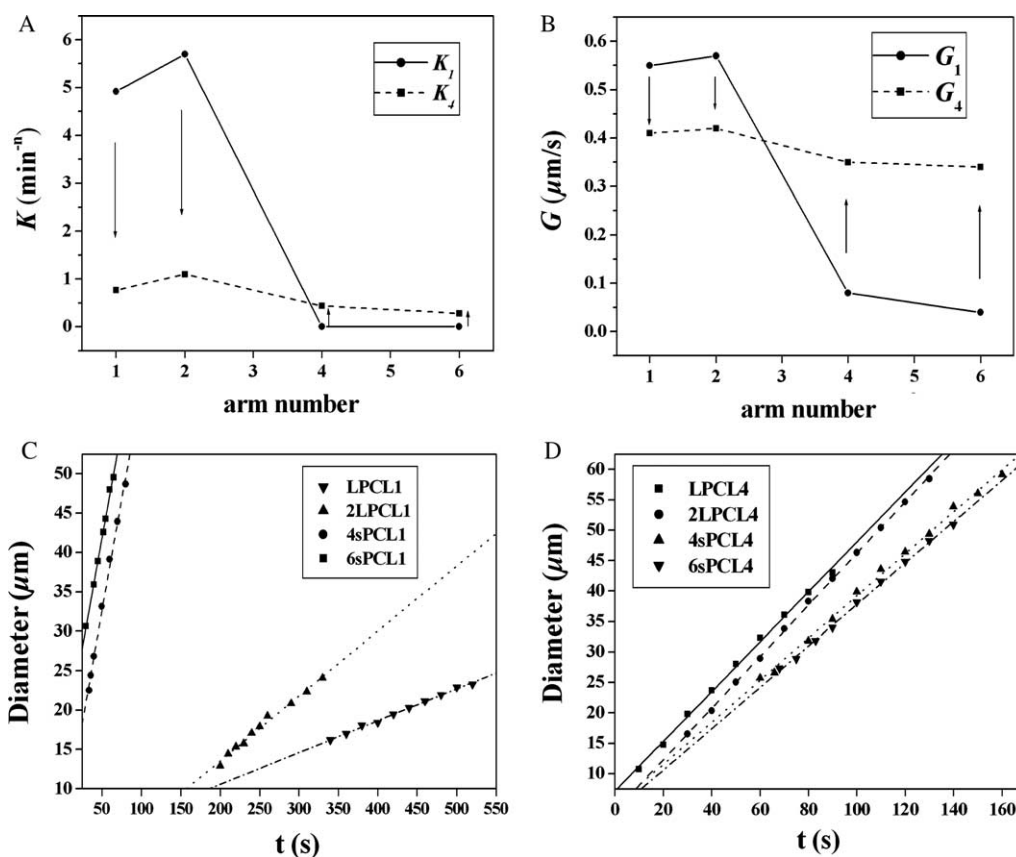


Fig. 4. (A) The dependence of isothermal crystallization kinetic constant on the arm number of PCL determined from DSC; (B) the dependence of spherulitic growth rate on the arm number of PCL determined from POM; (C) the dependence of spherulitic diameter on time for the PCL with a low molecular weight; (D) the dependence of spherulitic diameter on time for the PCL with a high molecular weight.

increases with the increasing molecular weight of polymer. This is attributed to the decreased arm density, inducing less hydrogen-bond interactions among star-shaped PCL polymers. The above indicates that both the number of polymer arms and the molecular weight of polymer controlled the isothermal crystallization rate constant of these PCL polymers. This will be further verified by the following polarized optical microscope (POM) analysis. In addition, the effect of both the number of polymer arms and the molecular weight of polymer on $t_{1/2}$ is similar to that for K .

3.3. Spherulitic growth and morphology

A polarized optical microscope was used to observe the crystalline morphology and to compare the spherulitic growth rate of these PCL polymers, as presented in Fig. 5. The isothermal crystallization temperature at 38 °C was chosen between T_c and T_{m2} for all samples. Both LPCL1 and 2LPCL1 presented good spherulitic morphology and Maltese-cross patterns at the crystallization of 80 s (Fig. 5(A) and (B)).

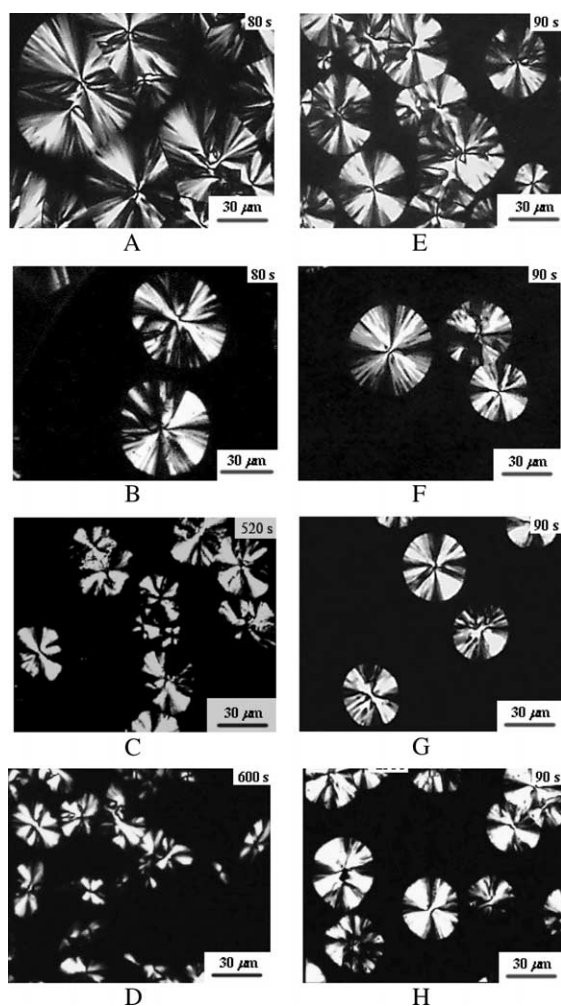
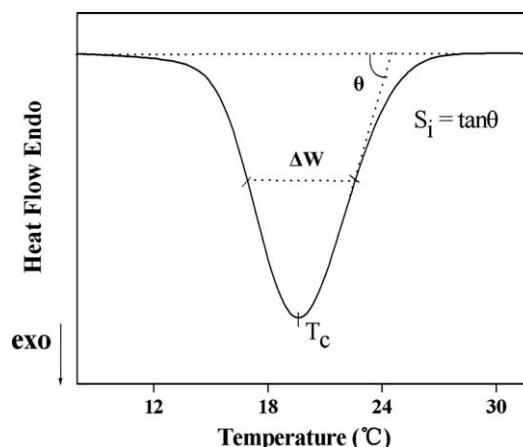


Fig. 5. POM photomicrographs of PCL crystallized at 38 °C: (A) LPCL1, 80 s; (B) 2LPCL1, 80 s; (C) 4sPCL1, 520 s; (D) 6sPCL1, 600 s; (E) LPCL4, 90 s; (F) 2LPCL4, 90 s; (G) 4sPCL4, 90 s; (H) 6sPCL4, 90 s.

However, both 4sPCL1 and 6sPCL1 showed irregular spherulites with poor morphology even at the crystallization time of 600 s (Fig. 5(C) and (D)). This indicates that the star-shaped architecture has an apparent effect on the morphology of the forming spherulites. With the increasing molecular weight of polymer, both 4sPCL4 and 6sPCL4 could give better spherulitic morphology and apparent Maltese-cross patterns even at the crystallization time of 90 s, which is similar to that observed in both LPCL4 and 2LPCL4 samples (Fig. 5(E)–(H)). Moreover, the average diameters of spherulites for these PCL polymers are plotted against isothermal crystallization time, as shown in Fig. 4(C) and (D). The diameter of spherulites linearly increases with isothermal crystallization time, and the spherulitic growth rate (G) was evaluated from the slope of these lines and listed in Table 3. From Fig. 4(B), it can be seen that the spherulitic growth rate is in the order of $G_{2LPCL} > G_{LPCL} > G_{4sPCL} > G_{6sPCL}$, and the effect of polymer molecular weight on G is also similar to that (the variation trend of K over the polymer molecular weight) determined in isothermal crystallization kinetics (Fig. 4(A)). In all, these results indicate that both the number of polymer arms and the molecular weight of polymer controlled the spherulitic morphology and the spherulitic growth rate, which is consistent with the analysis of isothermal crystallization kinetics.

3.4. Nonisothermal crystallization kinetics

It is important to investigate nonisothermal crystallization kinetics of these PCL polymers because polymer processing often proceeds under nonisothermal conditions. A typical DSC curve for the nonisothermal crystallization process during cooling from the melt is shown in Scheme 2. Fig. 6(A) exhibits the exothermic curves during the nonisothermal crystallization for LPCL1, 2LPCL1, 4sPCL1, and 6sPCL1 at various cooling rates ranging from 2 to 10 °C/min. Some useful parameters can be easily obtained to describe the nonisothermal crystallization behaviors of these PCL polymers: (1) the maximal crystallization temperature, T_c ; (2) the initial slope of the exotherm at



Scheme 2. Schematic representation of the parameters for nonisothermal crystallization process.

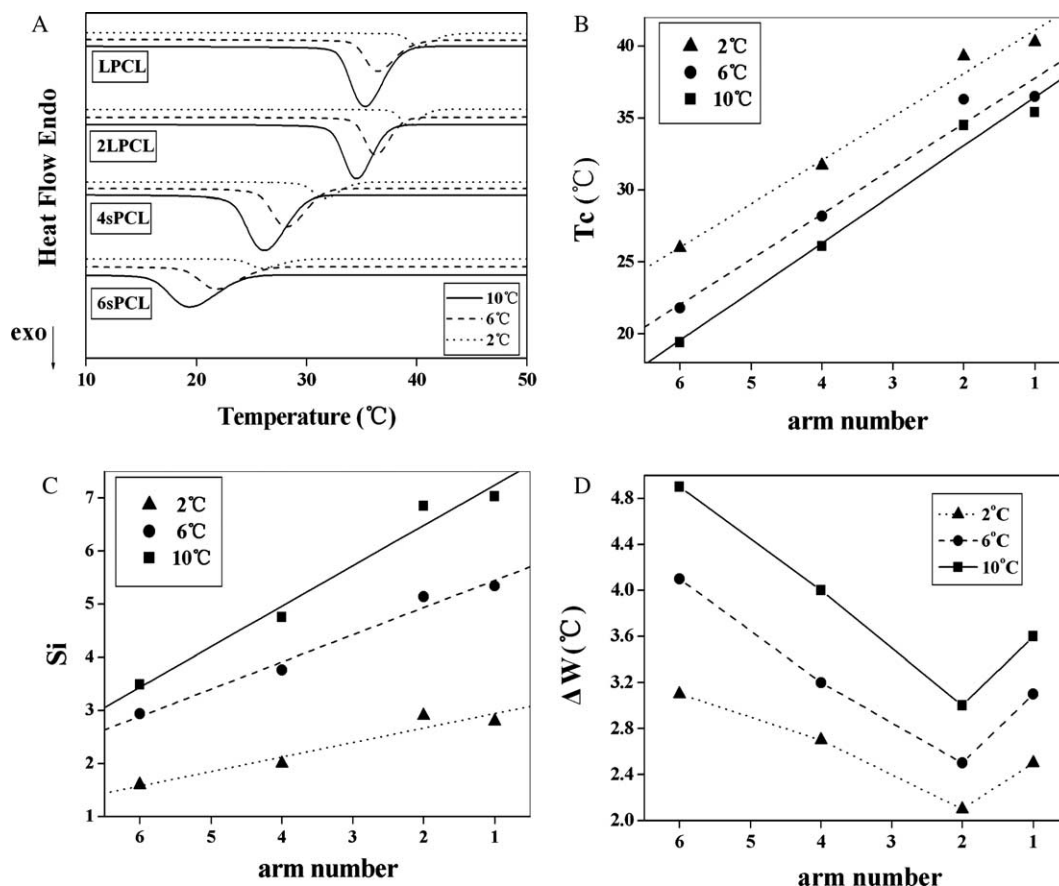


Fig. 6. (A) Nonisothermal crystallization exotherms of PCL at various cooling rates; (B) the dependence of T_c on the arm number of PCL at various cooling rates; (C) the dependence of S_i on the arm number of PCL at various cooling rates; (D) the dependence of ΔW on the arm number of PCL at various cooling rates.

Table 4
Nonisothermal crystallization kinetics parameters for the PCL polymers with different arms

Entry	Crystallization parameter	Cooling rate (°C/min)		
		2	6	10
6sPCL1	n		3.0	
	K'^a	8.22×10^{-3}	0.64	0.94
	$t_{1/2}$	1.98	1.01	0.95
	T_c (°C)	26.0	21.8	19.4
	ΔW (°C) ^b	3.1	4.1	4.9
	S_i^c	1.60	2.94	3.49
4sPCL1	n		3.1	
	K'^a	0.01	0.73	1.03
	$t_{1/2}$	1.86	0.99	0.94
	T_c (°C)	31.7	28.2	26.1
	ΔW (°C) ^b	2.7	3.2	4.0
	S_i^c	2.00	3.76	4.75
2LPCL1	n		3.6	
	K'^a	4.30×10^{-4}	1.02	1.14
	$t_{1/2}$	2.00	0.93	0.94
	T_c (°C)	39.3	36.3	34.5
	ΔW (°C) ^b	2.1	2.5	3.0
	S_i^c	2.90	5.14	6.85
LPCL1	n		3.5	
	K'^a	0.02	0.74	1.03
	$t_{1/2}$	1.77	0.99	0.95
	T_c (°C)	40.3	36.5	35.4
	ΔW (°C) ^b	2.5	3.1	3.6
	S_i^c	2.80	5.34	7.03

^a Nonisothermal crystallization rate constant (K') determined from Fig. 8.

^b ΔW denotes the width at half height of the exothermic peak (Scheme 2).

^c S_i denotes the initial slope of the exotherm at inflection on the high-temperature side (Scheme 2).

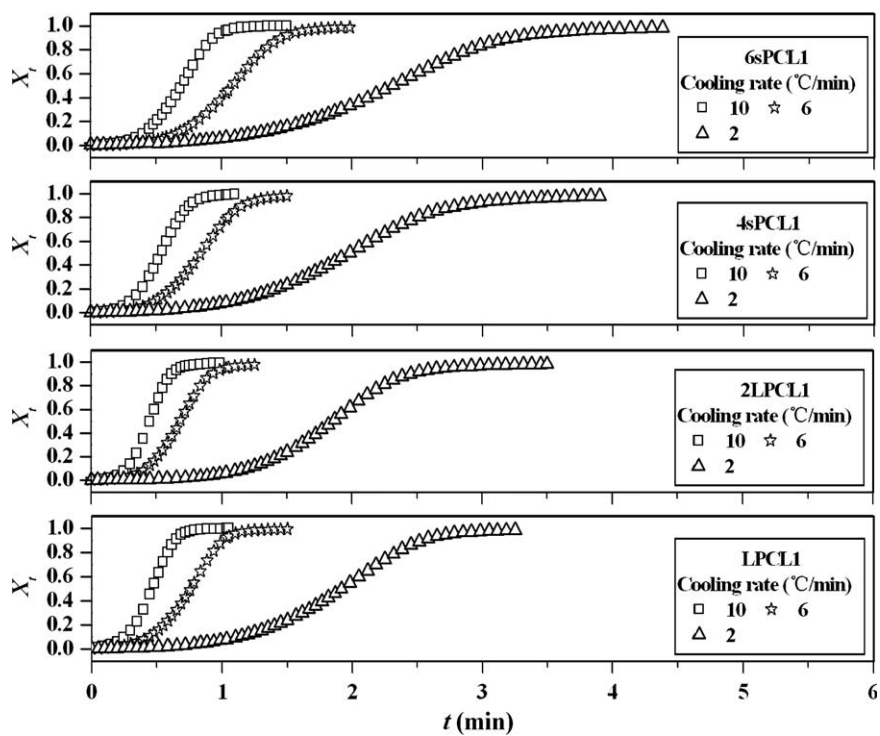


Fig. 7. Plots of relative degree of crystallinity (X_t) vs nonisothermal crystallization time (t) for PCL at various cooling rates.

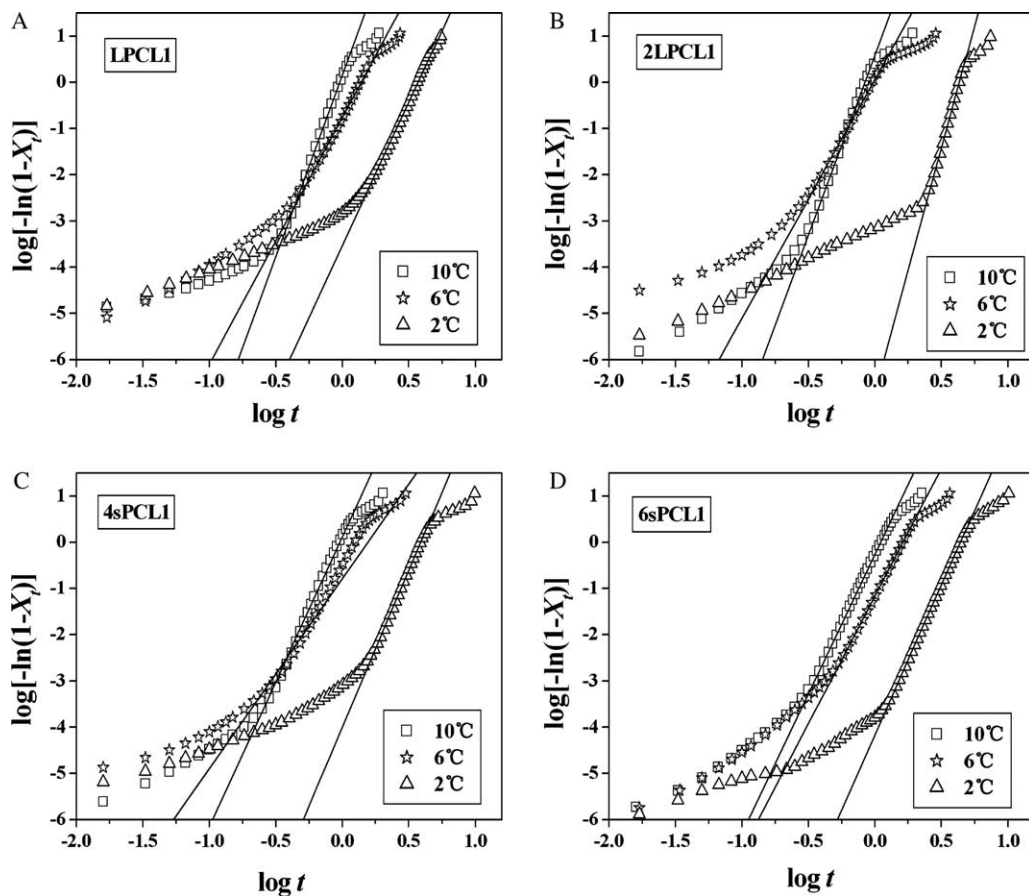


Fig. 8. Plots of $\log[-\ln(1-X_t)]$ vs $\log t$ for PCL during nonisothermal crystallization process: (A) LPCL1; (B) 2LPCL1; (C) 4sPCL1; (D) 6sPCL1.

inflection on the high-temperature side, S_i ; (3) the width at half height of the exothermic peak, ΔW , and the results are summarized in Table 4. It is clearly seen that T_c linearly increases with the decreasing arm number of PCL at a given cooling rate, and it is in the order of $T_{c,LPCL} > T_{c,2LPCL} > T_{c,4sPCL} > T_{c,6sPCL}$ (Fig. 6(B)). The S_i was employed to denote relative kinetics of the nonisothermal crystallization process, and higher absolute values of S_i suggest faster crystallization. From Fig. 6(C), it can be seen that the nonisothermal crystallization rate of PCL is in the order of $LPCL \approx 2LPCL > 4sPCL > 6sPCL$. The ΔW denotes the distribution of the forming crystal dimensions; i.e. the smaller the ΔW , the narrower the distribution. It can be seen that the distribution of the crystal dimensions is in the order of $\Delta W_{2LPCL} < \Delta W_{LPCL} < \Delta W_{4sPCL} < \Delta W_{6sPCL}$ at a given cooling rate, which is attributed to the molecular mobility induced by both the number of polymer arms and the constrained geometry of polymer. Moreover, the ΔW increases with the increasing cooling rate for each PCL, which suggests the increasing supercooling will cause the broader distribution of the crystal dimensions [29].

To thoroughly elucidate the nonisothermal crystallization kinetics, the nonisothermal crystallization exotherms in Fig. 6(A) are further analyzed by the modified Avrami–Ozawa method [38]. Fig. 7 shows the X_t (relative degree of crystallization) variations as a function of crystallization time. All curves present the similar S-shape, indicating that cooling rate has retardation effect on the crystallization of these PCL polymers. Moreover, the plots of $\log[-\ln(1-X_t)]$ vs $\log t$ were also shown in Fig. 8. From the slope and the intercept of the straight lines, the Avrami exponent, the nonisothermal crystallization rate constant (K'), and the crystallization half-time were estimated and compiled in Table 4. The Avrami exponent varied from 3.0 to 3.6 for these PCL polymers, suggesting that they crystallized in a three-dimensional growth mode with a heterogeneous nucleation. Furthermore, the nonisothermal crystallization rate constant has the variation trend of $K'_{2LPCL} > K'_{LPCL} > K'_{4sPCL} > K'_{6sPCL}$ when the cooling rate is high (such as 6 and 10 °C/min). This is consistent with that from the analyses of both isothermal crystallization kinetics and POM.

4. Conclusions

Both well defined star-shaped PCL having four arms (4sPCL) and six arms (6sPCL) and linear PCL having one arm (LPCL) and two arms (2LPCL) were successfully synthesized from the controlled ring-opening polymerization of CL using both commercial primary alcohols and SnOct₂ catalyst. The maximal melting point, the crystallization temperature, and the degree of crystallinity of these PCL polymers decrease with the increasing number of polymer arms, and they have similar crystalline structure. Both the isothermal and the nonisothermal crystallization rate constants of these PCL polymers are in the order of $K_{2LPCL} > K_{LPCL} > K_{4sPCL} > K_{6sPCL}$. Notably, the K of linear PCL decreases with the increasing molecular weight of polymer

while that of star-shaped PCL inversely increases. The variation trend of K over the number of polymer arms or the molecular weight of polymer is consistent with that of the spherulitic growth rate. Both star-shaped and linear PCL with a high molecular weight presented good spherulitic morphology and apparent Maltese-cross patterns. In all, both the number of polymer arms and the molecular weight of these PCL polymers controlled the isothermal and nonisothermal crystallization rate constants, the spherulitic growth rate, and the morphology.

Acknowledgements

The authors are greatly grateful for the financial support of the National Natural Science Foundation of China (20404007) and the Shanghai Science and Technology Committee of China (05DJ14005).

Supplementary data

Supplementary data associated with this article can be found at doi:10.1016/j.polymer.2006.02.047. The dependence of T_{m2} vs $M_{n,arm}$ and WAXD for the PCL polymers with different arms. This material is available from the authors.

References

- [1] Mecerreyes D, Jerome R, Dubois Ph. *Adv Polym Sci* 1999;147:1–59.
- [2] Eastmond GC. *Adv Polym Sci* 1999;149:59–223.
- [3] Sudesh K, Abe H, Doi Y. *Prog Polym Sci* 2000;25:1503–55.
- [4] Södergard A, Stolt M. *Prog Polym Sci* 2002;27:1123–63.
- [5] Albertsson AC, Varma IK. *Biomacromolecules* 2003;4:1466–86.
- [6] Breitenbach A, Pistel KF, Kissel T. *Polymer* 2000;41:4781–92.
- [7] Gillies ER, Frechet JMJ. *J Am Chem Soc* 2002;124:14137–46.
- [8] Cai Q, Zhao Y, Bei J, Wang S. *Biomacromolecules* 2003;4:828–34.
- [9] Rieger J, Bernaerts KV, Du Prez FE, Jerome R, Jerome C. *Macromolecules* 2004;37:9738–45.
- [10] Wang F, Bronich TK, Kabanov AV, Rauh RD, Roovers J. *Bioconjugate Chem* 2005;16:397–405.
- [11] Voit B. *J Polym Sci, Polym Chem* 2000;38:2505–25.
- [12] Astruc D, Chardac F. *Chem Rev* 2001;101:2991–3023.
- [13] Ihre H, Padilla De Jesus OL, Fréchet JMJ. *J Am Chem Soc* 2001;123:5908–17.
- [14] Gao C, Yan D. *Prog Polym Sci* 2004;29:183–275.
- [15] McKee MG, Wilkes GL, Long TE. *Prog Polym Sci* 2005;30:507–39.
- [16] Trollsas M, Hedrick JL. *J Am Chem Soc* 1998;120:4644–51.
- [17] Trollsas M, Claesson H, Atthoff B, Hedrick JL. *Angew Chem, Int Ed* 1998;37:3132–6.
- [18] Trollsas M, Atthoff B, Claesson H, Hedrick JL. *J Polym Sci, Polym Chem* 2004;42:1174–88.
- [19] Hecht S, Ihre H, Frechet JMJ. *J Am Chem Soc* 1999;121:9239–40.
- [20] Hecht S, Vladimirov N, Frechet JMJ. *J Am Chem Soc* 2001;123:18–25.
- [21] Kricheldorf HR, Hachmann-Thiessen H, Schwarz G. *Macromolecules* 2004;37:6340–5.
- [22] Sando F, Sanada H, Shibasaki Y, Endo T. *Macromolecules* 2002;35:680–3.
- [23] Dong CM, Qiu KY, Gu ZW, Feng XD. *Macromolecules* 2001;34:4691–6.
- [24] Dong CM, Qiu KY, Gu ZW, Feng XD. *Polymer* 2001;42:6891–6.
- [25] Dong CM, Qiu KY, Gu ZW, Feng XD. *J Polym Sci, Polym Chem* 2002;40:409–15.

- [26] Wang JL, Wang L, Dong CM. *J Polym Sci, Polym Chem* 2005;43:5449–57.
- [27] Burgath A, Sunder A, Neuner I, Mülhaupt R, Frey H. *Macromol Chem Phys* 2000;201:792–7.
- [28] Choi J, Kwak SY. *Macromolecules* 2003;36:8630–7.
- [29] Choi J, Kwak SY. *Macromolecules* 2004;37:3745–54.
- [30] Zhao YL, Cai Q, Jiang J, Shuai XT, Bei JZ, Chen CF, et al. *Polymer* 2002;43:5819–25.
- [31] Zhao YL, Shuai XT, Chen CF, Xi F. *Chem Mater* 2003;15:2836–43.
- [32] Zhao YL, Shuai XT, Chen CF, Xi F. *Chem Commun* 2004;(14):1608–9.
- [33] Zhao YL, Shuai XT, Chen CF, Xi F. *Macromolecules* 2004;37:8854–62.
- [34] Hao Q, Li F, Li Q, Li Y, Jia L, Yang J, et al. *Biomacromolecules* 2005;6:2236–47.
- [35] Tsuji H, Miyase T, Tezuka Y, Saha SK. *Biomacromolecules* 2005;6:244–54.
- [36] Youan BB, Benoit MA, Rollmann B, Riveau G, Gillard J. *J Microencapsulation* 1999;16:601.
- [37] Bittiger H, Marchessault RH. *Acta Crystallogr* 1970;B26:1923.
- [38] Weng W, Chen G, Wu D. *Polymer* 2003;44:8119–32.